CHIN. PHYS. LETT. Vol. 33, No. 1 (2016) 014301

Effects of Transverse Temperature Gradient on the Rotor Velocity in an Ultrasonic Motor *

Li-Ping Cheng(程利平)**, Shu-Yi Zhang(张淑仪), Xiao-Dong Xu(徐晓东)

Lab of Modern Acoustics, Institute of Acoustics, Nanjing University, Nanjing 210093

(Received 9 October 2015)

As a result of the nonlinear effect, acoustic streaming has been widely used for increasing the transport coefficient or driving a rotor, for example, in resonant cavities and non-contact ultrasonic motors. It has been demonstrated by experiments that a temperature gradient transverse to the wave propagating direction can significantly increase the velocity of the streaming flows in resonant cavities. To check whether the transverse temperature gradient can also increase the working velocity of acoustic streaming-driven motors, we investigate this issue by numerically solving the hydrodynamic equations. It is found that the velocity of the rotor only weakly depends on the transverse temperature gradient, e.g., even with a temperature difference of 40°C between the rotor and the stator, the velocity increases only ∼8.8%.

PACS: 43.25.Nm, 43.35.−c, 43.55.Ka DOI: 10.1088/0256-307X/33/1/014301

Motors are widely used in the mechanical, optical, electronic, and automatic industries and technologies.[1−3] Traditional ultrasonic motors are driven by the contact friction between the rotor and the stator. However, the contact friction between the rotor and the stator restricts the rotor velocity and the working lifetime of the motors.[4] To overcome these shortcomings, noncontact motors were proposed, where a fluid layer is located between the rotor and the stator.[5] As ultrasonic waves are excited in the stator and then propagate in the fluid, acoustic streaming is induced inside the fluid due to the nonlinear effect of acoustic waves, which drives the rotor to move. As explained in the classical textbook written by Landau *et al.*,[6] vortex flows form in the fluid when sound waves are affected by solid obstacles. On the one hand, the vortex flows can greatly increase the transport efficiency such as in heat conduction; on the other hand, such vortex flows can be used to drive a motor to move. Experiments have already confirmed the validity of this kind of acoustic streaming-driven noncontact motors.[7−9] With the angular frequency of the propagating wave on the surface of the stator, 1.65×10^5 rad/s, the wavelength 0.029 m, and the vibrating amplitude 4.3×10^{-6} m, Hu *et al.*[7] found that the mean velocity of the rotor is 970 rpm. Luchini *et al.* derived an analytical solution for the same phenomenon with the second-order approximation.[10] It turned out that the estimated velocity of the rotor would be five times smaller. Such a discrepancy was reconciled by Cheng *et al.*,[11] who performed two-dimensional (2D) hydrodynamic simulations. It was revealed that the experiments conducted by Hu *et al.*[7] can be reproduced perfectly. For example, with the same parameters as in the case B of Hu *et al.*,[7] the resulting free-rotor speed in our hydrodynamic simulations is very close to the experimental value, which implies that the acoustic streaming can account for the main part of the rotation, and the second-order approximation analytical solution may underestimate the rotor velocity considerably. Later, we further performed a parameter survey with numerical simulations,[12] and the results indicated that (i) the replacement of fixed viscosity by the temperature-dependent viscosity decreases the rotor velocity by ∼11%; (ii) heat conduction plays a trivial role; and (iii) the rotor velocity increases more and more rapidly as the thickness of the air gap between the stator and the rotor becomes smaller and smaller.

Later, it was found from experiments that inside a resonant cavity with an oscillating wall on one side, the velocity of the acoustic streaming is very sensitive to the transverse temperature gradient,[13] i.e., the temperature gradient normal to the direction of acoustic wave propagation. For example, by increasing the temperature difference ΔT from 0 to 0.3℃, the longitudinal velocity amplitude increases from 0.74 to 1.17 cm/s. Therefore, it will be very interesting to investigate whether the transverse temperature gradient can significantly increase the velocity of the noncontact ultrasonic motor. In this Letter, we first describe the numerical method, and then present our numerical results, which are discussed briefly at the end.

Figure 1(a) shows the schematic sketch of the noncontact motor, where the outer annulus is the stator and the inner annulus is the rotor, with air filling the gap in between. Ultrasonic waves are excited along the inner surface of the stator, along which they propagate. The radius of the rotor is R, and the thickness of the gap is h. As carried out by Luchini *et al.*[10] and

*Supported by the National Natural Science Foundation of China under Grant No 10874083.

**Corresponding author. Email: chenglp@nju.edu.cn

© 2016 Chinese Physical Society and IOP Publishing Ltd

Cheng *et al.*,[11] such an axisymmetric system is simplified in two parallel plates as depicted in Fig. 1(b), since h is much smaller than the perimeter of the stator. This approximation is validated since the comparison between the pure shear motions in the Cartesian and polar coordinates, in both of which analytical solutions can be obtained, indicating that such a simplification introduces a relative error of the order of $h/(8R)$, i.e., 2×10^{-4} in the present scenario.[11] Such a 2D model was investigated numerically by Cheng *et al.*[11,12]

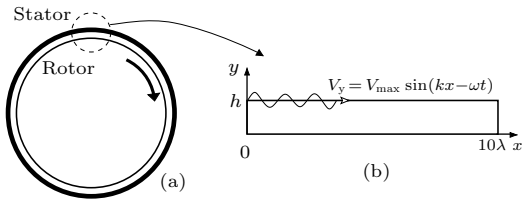

Fig. 1. (a) Schematic of the motor, and (b) the simulation box, where a propagating wave $V_y = V_{\max}\sin(kx-\omega t)$ is introduced at the top. Here $k = 2\pi/\lambda$ is the wave number.

The dynamics of the air in the simulation box is described by the full 2D continuity, Navier–Stokes, and energy equations for a compressible fluid. In the Cartesian coordinates, these equations which are numerically solved with the alternative direction implicit scheme, are expressed as follows:

$$\frac{\partial\rho}{\partial t} + \nabla\cdot(\rho\boldsymbol{v}) = 0, \tag{1}$$

$$\frac{\partial\boldsymbol{v}}{\partial t} + (\boldsymbol{v}\cdot\nabla)\boldsymbol{v} + \frac{1}{\rho}\nabla(\rho RT) - \frac{1}{\rho}\nabla\cdot(2\mu\boldsymbol{S}) - \frac{1}{\rho}\nabla\cdot\left(\frac{2}{3}\mu\nabla\cdot\boldsymbol{v}\right) = 0, \tag{2}$$

$$\frac{\partial T}{\partial t} + \boldsymbol{v}\cdot\nabla T - Q - \frac{\phi}{\rho c_{\rm v}} + (\gamma-1)T\nabla\cdot\boldsymbol{v} = 0, \tag{3}$$

where $R = 287\,\text{Pa/kg}$ is the specific gas constant, T is the temperature, t is the time, μ is the first coefficient of dynamic viscosity, $c_{\rm v}$ is the specific heat at the constant volume, γ is the ratio of specific heat of the gas (for the air, $\gamma = 1.4$), $\boldsymbol{S}$ is the strain rate tensor, ϕ is the viscous dissipation function, and $Q = 1/(\rho c_{\rm v})\nabla\cdot(\kappa\nabla T)$ is the thermal conduction term, with κ being the thermal conductivity. In our simulations, the temperature-dependent viscosity and thermal conductivity are taken into account by using

$$\mu(T) = \mu_0\left(\frac{T}{T_1}\right)^{1.5}\frac{T_1+T_{\rm s}}{T+T_{\rm s}}, \tag{4}$$

$$\kappa(T) = (5.22+0.07T)\times10^{-3}, \tag{5}$$

where μ_0 is the dynamic viscosity at 0℃, T_1 and $T_{\rm s}$ are equal to 273.16 K and 110.4 K, respectively. Equation (4) is the Sutherland formula.

The hydrodynamic equations (1)–(3) are nondimensionalized by using the following characteristic values: T_0 (the initial temperature) for the temperature, $\rho_0{=}p_0/RT_0$ for the density, where p_0 is the standard atmospheric pressure, the isothermal sound speed $v_0 = \sqrt{RT_0}$ for the velocity, h for the space, and $\tau_0{=}h/v_0$ for the time. As the initial conditions, a uniform isothermal gas is assumed to be static, i.e., $T{=}1$, $\rho{=}1$, and $v = 0$. The horizontal size of the simulation box is taken to be ten times the wavelength (λ) of the acoustic wave on the stator. However, three cases with different vertical sizes are simulated, i.e., $h = 30\,\mu$m, $50\,\mu$m, and $100\,\mu$m. Correspondingly, whereas the dimensionless thickness of the simulation box is always 1, the dimensionless widths are 9787, 5872, and 2936, respectively. The domain is discretized by 82×581 grid points, which are uniformly distributed in both directions. Periodic conditions are applied to the left and the right boundaries. On the top boundary, a freely propagating transverse wave is specified, where $u = 0$ and $v = 0.71\sin(kx-\omega t)/v_0$, ρ is determined by extrapolation, and $T = 1$ is fixed. Here $k = 2\pi/\lambda$ is the wave number, with $\lambda = 0.029\,$m, and $\omega = 1.65\times10^5\,$rad/s is the angular frequency. The bottom boundary, which corresponds to the rotor, is assumed to be a freely rotating wall. To clarify how the transverse temperature gradient can change the rotor velocity, the temperature at the bottom is fixed at $T = 1+\Delta T/T_0$, where ΔT is a free parameter.

The evolution of the air filling the gap is basically the same as in Ref. [11], which is described briefly as follows: as ultrasonic waves propagate rightward along the top boundary, acoustic waves are excited in air. Owing to the nonlinear effect, the propagating acoustic waves generate a net flow moving to the right, i.e., the average velocity of any spatial point over a period is nonzero. The velocity of the net flow increases nearly monotonically from the top to the bottom, reaching the maximum near the bottom, where the rotor is located. With the parameters $h = 50\,\mu$m and $\Delta T = 0$, the saturation velocity of the rotor is 1.6 m/s.

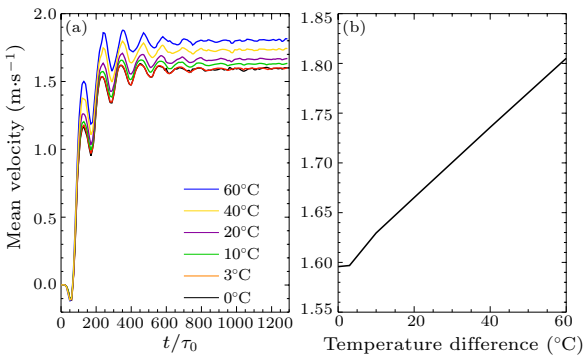

Fig. 2. (a) Time evolution of the rotor velocity in six cases with different temperature gradients. (b) Dependence of the saturation velocity of the rotor on the temperature gradient. The thickness of the air gap is at $h = 50\,\mu$m in these cases.

To check whether the temperature difference between the bottom and the top can affect the saturation velocity of the rotor (v_r), five other cases are simulated, with $\Delta T = 3$, 10, 20, 40, 60℃. Note that the thickness of the air gap is fixed at $h = 50\,\mu$m. Figure 2(a) displays the temporal evolution of the rotor velocity in the total six cases. It is seen that all of them show similar evolution profiles, while the saturation velocity increases slightly except in the case of $\Delta T = 3$℃, where the velocity profile is almost identical to the case of $\Delta T = 0$℃. The variation of the saturation velocity of the rotor along with the temperature gradient is depicted in Fig. 2(b). It is found that as ΔT increases, v_r increases almost linearly but quite slowly. For example, even when $\Delta T = 40$℃, v_r reaches only 1.74 m/s, which is increased by ∼8.8% compared with the case with $\Delta T = 0$℃.

Considering that the thickness of the air gap might influence the effect of the temperature difference on the rotor velocity, cases with $h = 30\,\mu$m and $100\,\mu$m are also simulated. It is revealed that as ΔT increases from 0℃ to 40℃, the rotor velocity increases 8.0% for the case with $h = 30\,\mu$m and by 5.1% for the case with $h = 100\,\mu$m, both of which are slightly weaker than the case with $h = 50\,\mu$m. It seems that for any thickness of the air gap, the working velocity of our rotor is insensitive to the transverse temperature gradient.

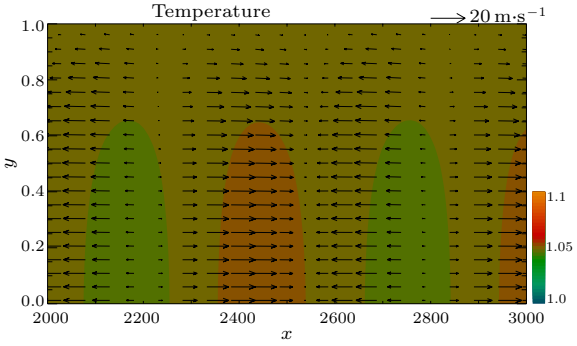

Fig. 3. The distributions of the temperature (color) and the velocity field (arrows) when the flow becomes steady in the case without the transverse temperature gradient. The velocity field does not show any eddy structure. The arrow above the panel indicates the velocity scale.

For the hydrodynamics inside a resonant cavity, it is found that the transverse temperature gradient can significantly increase the acoustic streaming, for example, even with a temperature difference of 0.3℃, the velocity of the acoustic streaming is increased by 58%.[13] However, in the case of the motors driven by the acoustic streaming, our numerical simulations reveal that the amplitude of the acoustic streaming velocity only increases slightly with the transverse temperature gradient, e.g., even with a temperature difference of 40℃, the rotor velocity increases only 8.8%. This result shows that the performance of the acoustic streaming-driven motors runs very stably. Not only is it weakly dependent on the environmental temperature,[12] but also it changes slightly with the temperature difference between the rotor and the stator.

It is interesting to see the completely different effects of the transverse temperature gradient on the acoustic streaming velocity for the motors and for the resonant cavities. A possible reason is that the acoustic streaming in the resonant cavities forms a series of vortices as revealed by Lin *et al.*[14] and Nabavi *et al.*,[13] where standing acoustic waves are imposed as carried out by Nadal *et al.*[15] The temperature difference between the top and the bottom boundaries easily distorts the symmetry of the vortices, making two symmetric vortices collapse into one. In our case, however, there are no vortices in the air gap, and the flow pattern remains very stable, not fragile to the transverse temperature gradient. Figure 3 shows the distributions of the gas temperature (color scales) and the velocity field (arrows) when the evolution is steady in the case without the transverse temperature gradient. Note that the velocity field is oscillating, and it is the net value of the oscillating velocity that corresponds to the acoustic streaming flow. It is seen that there is no vortex in the flow pattern in the cases either without or with the transverse temperature gradient. Actually, both the oscillating velocity and the net velocity are mainly shear flows in the x-direction, showing no clear vortex cells that were present in Ref. [13].

In summary, with hydrodynamic numerical simulations, we conclude that the transverse temperature gradient has a very weak effect on the net flow velocity in the acoustic streaming used to drive motors as designed by Hu *et al.*[7] (see our Fig. 1).

References

[1] Sashida T and Kenjo T 1993 *An Introduction to Ultrasonic Motors* (Oxford: Clarendon)
[2] Zhao C 2007 *Ultrasonic Motors Technologies and Applications* (Beijing: Science Press)
[3] Lei H and Tan X Q 2015 *Chin. Phys. Lett.* **32** 027302
[4] Hu J H, Nakamura K and Ueha S 1996 *Jpn. J. Appl. Phys.* **35** 3289
[5] Yang B, Liu J Q, Chen D and Cai B C 2005 *Chin. Phys. Lett.* **22** 2598
[6] Landau D and Lifschitz E M 1986 *Theory of Elasticity* (New York: Pergamon)
[7] Hu J, Nakamura K and Ueha S 1997 *Ultrasonics* **35** 459
[8] Gu H H, Zhang S Y, Cheng L P, Ma D, Zhou F M, Chen Z J and Shui X J 2009 *Sens. Actuators* A **155** 163
[9] Cheng L P, Zhang S Y, Gu H H, Zhou, F M and Shui X J 2010 *Chin. Phys. Lett.* **27** 074302
[10] Luchini P and Charru F 2005 *Phys. Fluids* **17** 122106
[11] Cheng L P and Zhang S Y 2007 *Appl. Phys. Lett.* **90** 244106
[12] Cheng L P and Zhang S Y 2009 *J. Appl. Phys.* **106** 074506
[13] Nabavi M, Siddiqui K and Dargahi J 2008 *Appl. Phys. Lett.* **93** 051902
[14] Lin Y Q and Farouk B 2008 *Int. J. Heat Mass Transfer* **51** 3179
[15] Nadal F and Lauga E 2014 *Phys. Fluids* **26** 082001